Tau can switch microtubule network organizations: from random networks to dynamic and stable bundles

Elea Prezel[a,b,†], Auréliane Elie[a,b,†], Julie Delaroche[a,b], Virginie Stoppin-Mellet[a,b], Christophe Bosc[a,b], Laurence Serre[a,b,c], Anne Fourest-Lieuvin[a,b,d], Annie Andrieux[a,b,d], Marylin Vantard[a,b,c], and Isabelle Arnal[a,b,c,*]

[a]Inserm, U1216, [b]Grenoble Institut des Neurosciences, Université Grenoble Alpes, [c]Centre National de la Recherche Scientifique, Grenoble Institut des Neurosciences, and [d]Commissariat à l'Energie Atomique et aux Energies Alternatives, Institut de Biosciences et Biotechnologies de Grenoble, F-38000 Grenoble, France

ABSTRACT **In neurons, microtubule networks alternate between single filaments and bundled arrays under the influence of effectors controlling their dynamics and organization. Tau is a microtubule bundler that stabilizes microtubules by stimulating growth and inhibiting shrinkage. The mechanisms by which tau organizes microtubule networks remain poorly understood. Here, we studied the self-organization of microtubules growing in the presence of tau isoforms and mutants. The results show that tau's ability to induce stable microtubule bundles requires two hexapeptides located in its microtubule-binding domain and is modulated by its projection domain. Site-specific pseudophosphorylation of tau promotes distinct microtubule organizations: stable single microtubules, stable bundles, or dynamic bundles. Disease-related tau mutations increase the formation of highly dynamic bundles. Finally, cryo–electron microscopy experiments indicate that tau and its variants similarly change the microtubule lattice structure by increasing both the protofilament number and lattice defects. Overall, our results uncover novel phosphodependent mechanisms governing tau's ability to trigger microtubule organization and reveal that disease-related modifications of tau promote specific microtubule organizations that may have a deleterious impact during neurodegeneration.**

Monitoring Editor
Xueliang Zhu
Chinese Academy of Sciences

Received: Jun 30, 2017
Revised: Nov 8, 2017
Accepted: Nov 13, 2017

INTRODUCTION

The microtubule cytoskeleton is responsible for vital cellular processes such as cell division, morphogenesis, and differentiation. Microtubules are 25-nm-diameter hollow cylinders composed of a lattice made up of α-β-tubulin heterodimers aligned head-to-tail to form protofilaments (Amos and Schlieper, 2005). Microtubules are constantly remodeled through alternating growth and shrinkage of their extremities, a behavior known as dynamic instability (Mitchison and Kirschner, 1984). In neurons, microtubules serve as tracks for organelle transport and can be found as single polymers or as linear bundles (Conde and Cáceres, 2009; Kapitein and Hoogenraad, 2015). Populations of stable microtubule bundles are thought to ensure axon consolidation and maintenance. However, several studies have indicated that microtubules within bundles retain some of their dynamic properties, which are crucial to axon outgrowth, guidance, branching, and regeneration (Hoogenraad and Bradke, 2009; Voelzmann *et al.*, 2016). The unique organizations of neuronal microtubules depend on a variety of microtubule-associated proteins (MAPs) that control microtubule assembly, dynamics, severing, and bundling, as well as interaction with organelles.

Tau is a major neuronal MAP involved in the regulation of microtubule bundling and dynamics (Weingarten *et al.*, 1975; Cleveland *et al.*, 1977a,b; Binder *et al.*, 1985; Chen *et al.*, 1992; Drechsel *et al.*, 1992; Brandt and Lee, 1993b; Trinczek *et al.*, 1995). As tau plays a role in Alzheimer's disease and related dementias, where it

This article was published online ahead of print in MBoC in Press (http://www.molbiolcell.org/cgi/doi/10.1091/mbc.E17-06-0429) on November 22, 2017.

†These authors contributed equally to this work.

*Address correspondence to: Isabelle Arnal (isabelle.arnal@univ-grenoble-alpes.fr).

Abbreviations used: MAP, microtubule-associated protein; MTBD, microtubule-binding domain; PHF, paired helical filaments.

aggregates in paired helical filaments (PHFs) in response to modifications such as phosphorylation, truncation, or mutations, it has been extensively studied (Ingram and Spillantini, 2002; Gendron and Petrucelli, 2009; Kolarova *et al.*, 2012; Fitzpatrick *et al.*, 2017). How these pathological forms of tau affect cytoskeletal organization remains a subject of debate, but it could involve detachment of tau from microtubules due to aggregation and/or alterations of tau's microtubule-regulating properties (Alonso *et al.*, 1994; Elbaum-Garfinkle *et al.*, 2014).

Tau is an intrinsically disordered protein consisting of an acidic N-terminal projection domain, a microtubule-binding domain (MTBD) including three or four repeated motifs (R1 to R4), and a C-terminal tail (Figure 1A). Alternative splicings of tau produce six isoforms that differ by the length of the projection domain and the

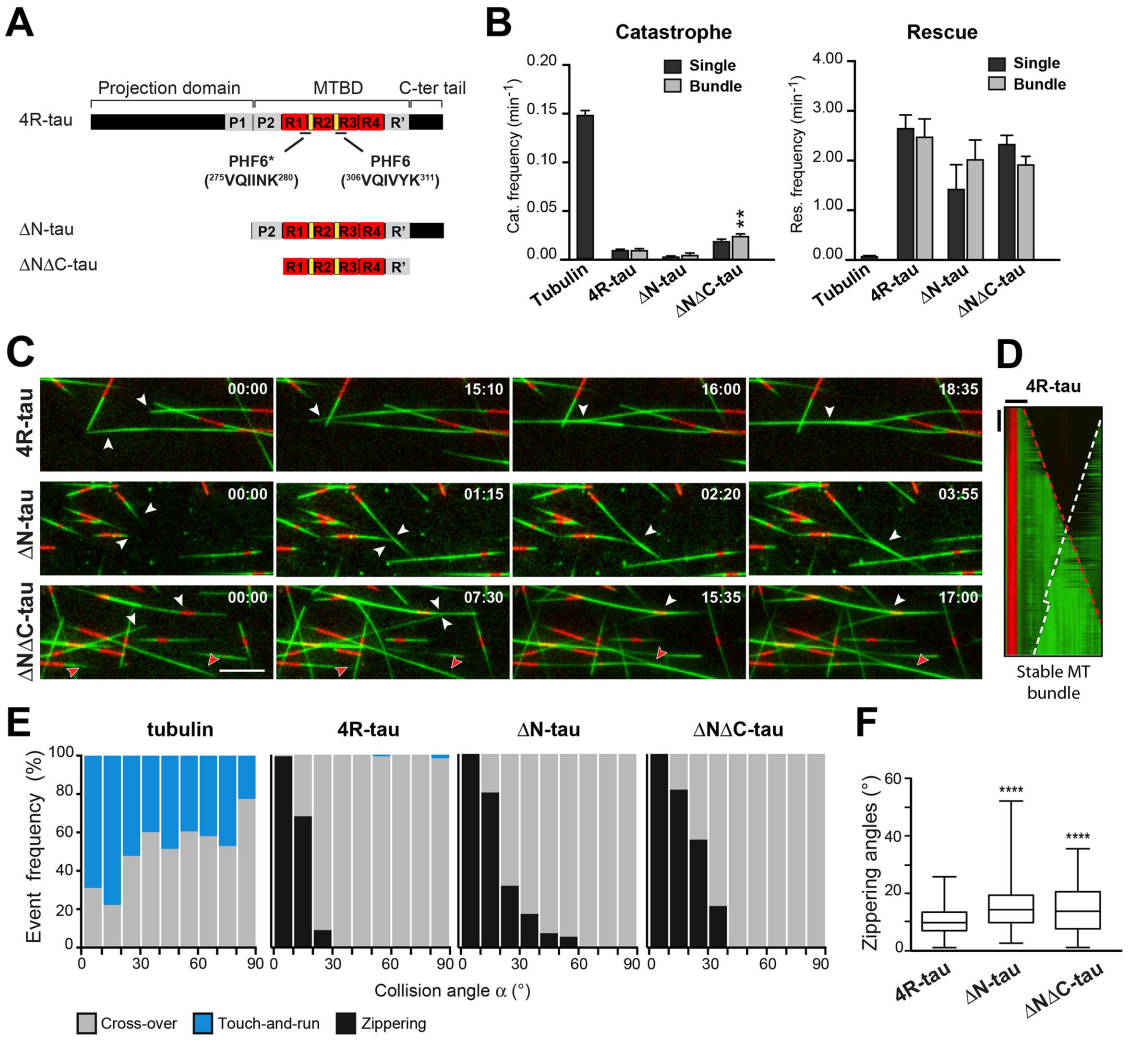

FIGURE 1: The projection domain of tau modulates tau's capacity to bundle microtubules. (A) Schematic representation of 4R-tau and deletion mutants (ΔN- and ΔNΔC-tau). Tau consists of an N-terminal projection domain, a microtubule-binding domain (MTBD), and a C-terminal tail. The projection domain includes the N-terminal part of the protein and the proline-rich domain P1. The MTBD is composed of a proline-rich domain (P2), four repeats (R1 to R4), and one pseudo-repeat (R'). The two conserved hexapeptides PHF6* and PHF6 are located at the beginning of R2 and R3, respectively. (B) Effects of full-length and truncated tau proteins on frequency of catastrophes (left) and rescues (right) in single and bundled microtubules (see Supplemental Table S1 for detailed values). Microtubules were assembled from 10 μM tubulin in the presence of 100 nM 4R-tau, ΔN-tau or ΔNΔC-tau. $^{**}p < 0.01$ (Kruskal–Wallis analysis of variance [ANOVA] followed by a post hoc Dunn's multiple comparison). *p* values were calculated relative to the 4R-tau condition. (C) TIRF microscopy time series of microtubules growing in the presence of 4R-, ΔN-, and ΔNΔC-tau. White and red arrowheads indicate two distinct microtubule bundling events. Time is indicated in min:s. Scale bars, 10 μm. (D) Kymograph example of microtubules growing in the presence of 4R-tau and forming a stable microtubule bundle. Dotted lines represent the growing extremities of microtubules. Horizontal scale bars: 10 μm; vertical scale bars: 3 min. MT, microtubule. (E) Frequency distributions of crossover (gray), touch-and-run (blue), and zippering (black) events as a function of microtubule collision angles in the presence of 4R-, ΔN-, and ΔNΔC-tau. At least 200 collision events were analyzed for each condition. (F) Distribution of collision angles at which microtubules coalign and zipper in the presence of 4R-tau, ΔN-tau, and ΔNΔC-tau. Boxes represent percentiles 25–75, and whiskers extend from the minimum to the maximum values. The horizontal lines inside boxes indicate median values. $^{****}p < 0.0001$ (Kruskal–Wallis ANOVA followed by post hoc Dunn's multiple comparison; the numbers of angles measured were 240, 106, and 123 for 4R-tau, ΔN-tau, and ΔNΔC-tau, respectively). *p* values are calculated in comparison to the 4R-tau condition.

number (three or four) of repeats (Himmler *et al.*, 1989; Goedert and Jakes, 1990). Tau interacts with microtubules through multiple binding hotspots located in its MTBD. Among them, two conserved hexapeptides, PHF domains (Figure 1A), are important for tau aggregation in Alzheimer's disease. These PHF domains can fold into hairpin-like structures when tau interacts with microtubules to stabilize a unique microtubule-bound conformation (Kadavath *et al.*, 2015). The MTBD also drives the microtubule-stabilizing activity of tau by stimulating microtubule growth and inhibiting microtubule shrinkage (Lee *et al.*, 1989; Goode and Feinstein, 1994; Goode *et al.*, 1997; Gustke *et al.*, 1994; Mukrasch *et al.*, 2009). The projection domain of tau has been proposed to trigger microtubule bundling via complete antiparallel dimerization (Rosenberg *et al.*, 2008; Feinstein *et al.*, 2016) or transient charge-charge attractions (Chung *et al.*, 2016), although other studies suggest that this domain is not required for microtubule bundling (Brandt and Lee, 1993a; Gustke *et al.*, 1994). To date, despite extensive study of tau interaction with single microtubules, the mechanisms by which normal and pathological forms of tau organize microtubule networks remain poorly understood.

In this paper, we describe in vitro self-organization of growing microtubules in the presence of various tau isoforms, fragments, and mutants. Our results show that the ability of tau to promote stable microtubule bundles depends on the two PHF sequences present in tau repeat motifs and is regulated by tau's projection domain. Importantly, site-specific pseudo-phosphorylation of tau differentially modulates its capacity to either bundle or stabilize microtubules, resulting in distinct network organizations: stable single microtubules, stable bundles, or dynamic bundles. We also identify two disease-relevant mutations of tau that abnormally enhance the formation of bundles composed of highly dynamic microtubules. Cryo–electron microscopy observations reveal that tau and its variants induce changes in the microtubule lattice by increasing the protofilament number and generating lattice defects. Overall, our work sheds light on novel molecular mechanisms by which normal and disease-related forms of tau differentially modulate microtubule bundling and dynamics to control microtubule network organizations.

RESULTS

The tau projection domain regulates its capacity to bundle microtubules

To investigate how tau affects the assembly and properties of microtubule bundles in vitro, we performed total internal reflection fluorescence (TIRF)–based assays of microtubules nucleated from randomly oriented short seeds in the presence of pure tubulin (10 μM) and tau proteins or fragments (100 nM) (Figure 1A). Collision events between growing microtubules were classified in three categories: 1) cross-over, 2) touch-and-run, and 3) coalignment followed by zippering and bundling (Supplemental Figure S1). To determine the bundling capacity of tau proteins, we analyzed the frequency of each event category for different microtubule collision angles. In parallel, the parameters of microtubule dynamic instability were determined for both single and bundled microtubules.

Compared with tubulin alone, full-length 4R-tau strongly inhibited catastrophes (transition from growth to shrinkage) and promoted rescues (transition from shrinkage to growth). This finding is consistent with 4R-tau's known microtubule-stabilizing activity (Figure 1B and Supplemental Table S1) (Panda *et al.*, 1995, 2003; Trinczek *et al.*, 1995). 4R-tau also induced the formation of bundles that were absent in the control (Figure 1, C–E, and Supplemental Movie S1); it frequently coaligned and zippered microtubules when they met at shallow angles (<25°) (Figure 1, E and F). At steeper angles, microtubules formed crossovers or very rarely touch-and-run events. Furthermore, tau-induced bundled microtubules displayed dynamic properties similar to those of single microtubules (Figure 1B and Supplemental Table S1), with bundles composed of stably growing microtubules (referred to as stable microtubule bundles; Figure 1D).

To investigate the roles played by the projection domain and the C-terminal tail of tau in microtubule bundling and dynamics, we produced two fragments: one in which the projection domain was deleted (ΔN-tau), and the other deleted for the projection domain and additional flanking regions of the MTBD (proline-rich domain P2 and C-terminal tail, ΔNΔC-tau) (Figure 1A). The two fragments continued to promote microtubule elongation and stabilization (Figure 1B and Supplemental Table S1) and to bundle microtubules (Figure 1, C and D, and Supplemental Movie S2). Compared with 4R-tau, ΔN- and ΔNΔC-tau enhanced the frequency of microtubule bundling per collision angle and extended the range of angles at which microtubule bundling occurred with angles up to 50° and 35°, respectively (Figure 1E). Owing to this effect, the median bundling angle increased significantly from 9° for the full-length 4R-tau to around 14° for the truncated forms (Figure 1F; see also Supplemental Movie S2). These results indicate that ΔN- and ΔNΔC-tau bundle microtubules more efficiently than full-length 4R-tau.

Overall, our data indicate that full-length tau is an active cross-linker promoting the formation of stable microtubule bundles. The repeat motifs in tau MTBD are sufficient to induce microtubule cross-linking, as suggested by earlier studies (Scott *et al.*, 1992; Brandt and Lee, 1993a). We also show that removal of the N-terminal projection domain of tau stimulates its microtubule bundling capacity.

The PHF domains are key elements in the formation of stable microtubule bundles

We next examined whether tau MTBD regulates microtubule bundling in addition to its role in microtubule binding and stabilization (Trinczek *et al.*, 1995; Mukrasch *et al.*, 2009). To do this, we produced various tau mutants lacking one or two repeats or both PHF domains, as these domains have recently been found to play a major role in determining the microtubule-bound conformation of tau (Figure 2A) (Kadavath *et al.*, 2015).

We first determined the ability of these tau variants to bind polymerizing microtubules at the same tau:tubulin ratio as the one used in our TIRF-based experiments, using cosedimentation assays as described previously (LeBoeuf *et al.*, 2008; Kiris *et al.*, 2011). We showed that all constructs interacted with microtubules to similar extents (Supplemental Figure S2), which supports the implied role of the repeat motifs and their flanking regions in microtubule binding (Mukrasch *et al.*, 2007). Because of this result, we are confident that the differences subsequently observed in the microtubule-regulating activities of tau constructs (microtubule bundling and/or stabilization) are due to inherent mechanistic differences and not to variations in their binding stoichiometry to microtubules. In vitro TIRF reconstitution showed that 3R-tau produced microtubule bundles with an efficiency almost comparable to that of 4R-tau, whereas 2R-tau exhibited very weak bundling activity (Supplemental Movie S3). Detailed analysis of bundling angle distributions indicated no major differences between 3R- and 4R-tau, whereas 2R-tau dramatically reduced both the probability of microtubule bundling per collision and the median bundling angle (Figure 2, B and C). Touch-and-run events were observed with 3R-tau and more frequently with 2R-tau (Figure 2B, in blue). This result correlates with the weaker microtubule

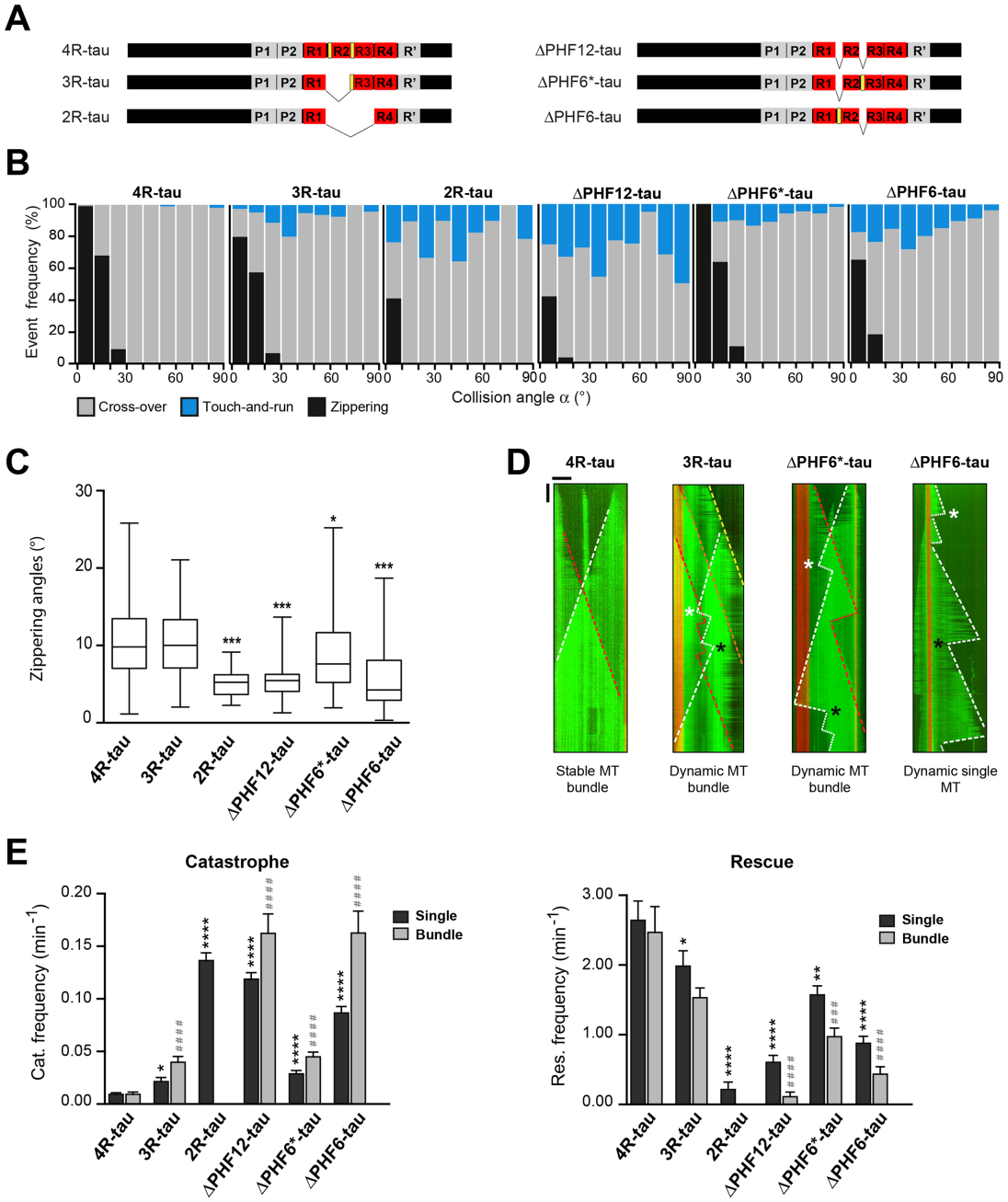

FIGURE 2: PHF sequences at the beginning of R2 and R3 are required for tau's microtubule-bundling and -stabilizing functions. (A) Schematic representation of 4R-tau and tau proteins lacking one repeat (3R-tau), two repeats (2R-tau), or the PHF domains (ΔPHF12-, ΔPHF6*-, and ΔPHF6-tau). Domain details are as in Figure 1A. (B) Frequency of crossover (gray), touch-and-run (blue), and zippering (black) events as a function of microtubule collision angles in the presence of the different tau proteins. Microtubules were assembled from 10 µM tubulin in the presence of 100 nM tau proteins. At least 200 collision events were analyzed for each condition. (C) Distribution of collision angles at which microtubules coalign and zipper in the presence of tau proteins. Boxes represent percentiles 25–75, and whiskers extend from the minimum to the maximum values. The horizontal lines inside boxes indicate median values. *$p < 0.05$, ***$p < 0.001$ (Kruskal–Wallis ANOVA followed by post hoc Dunn's multiple comparison; the numbers of angles measured were 240, 128, 14, 24, 66, and 137 for 4R-, 3R-, 2R-, ΔPHF12-, ΔPHF6-, and ΔPHF6*-tau, respectively). *p* values were calculated relative to the 4R-tau condition. (D) Kymograph examples of microtubules growing in the presence of distinct tau proteins (4R-, 3R-, ΔPHF6*-, and ΔPHF6-tau) producing different microtubule populations. Dotted lines represent the growing extremities of microtubules. White and black asterisks indicate some catastrophe and rescue events, respectively. Horizontal scale bars: 10 µm; vertical scale bars: 3 min. MT, microtubule. (E) Effects of tau proteins on the frequency of catastrophes (left) and rescues (right) for single and bundled microtubules (see SupplementalTable S1 for detailed values). For 2R-tau, dynamical parameters were determined only for single microtubules because microtubule bundles were too scarce. *$p < 0.05$, **$p < 0.01$, ****$p < 0.0001$, ###$p < 0.001$, ####$p < 0.0001$ (Kruskal–Wallis ANOVA followed by post hoc Dunn's multiple comparison). *p* values were calculated relative to single (*) or bundled (#) microtubules polymerized in the presence of 4R-tau.

stabilization (more catastrophes and fewer rescues) exerted by tau containing a reduced number of repeats (Figure 2E and Supplemental Table S1; also see Supplemental Movie S3; Trinczek *et al*., 1995). Thus 3R-tau produces bundles composed of dynamic microtubules (referred to as dynamic microtubule bundles, Figure 2D), whereas 2R-tau mainly produces single dynamic microtubules. Interestingly, in the presence of a tau mutant lacking the two PHF sequences (ΔPHF12-tau), growing microtubules behaved similarly to microtubules assembled with 2R-tau: they were highly dynamic and underwent very few coalignments, and those only at acute collision angles (<13°) (Figure 2, B, C, and E, and Supplemental Movie S3).

To test whether the highly dynamic behavior of microtubules assembled with 2R- or ΔPHF12-tau might alter the formation of microtubule bundles, we performed experiments at a higher tubulin concentration (17 μM) to ensure the production of longer, less dynamic polymers (Supplemental Figure S3 and Supplemental Movie S4). Under these conditions, a strong reduction of both microtubule bundling frequencies and median values of bundling angles was still observed in the presence of 2R- and ΔPHF-12-tau compared with 4R-tau. These data indicate that the two central repeats or the PHF sequences are essential to tau's capacity to bundle microtubules, and that this role is independent of the dynamic characteristics of microtubules.

We next examined whether the two PHF sequences exhibited a distinct regulating activity in microtubule bundling and stabilization. Deletion of the PHF domain in R2 (ΔPHF6*-tau, Figure 2A) decreased microtubule stabilization (to a similar extent to that observed with 3R-tau, Figure 2, D and E) but induced no major changes in microtubule bundling from 4R-tau (Figure 2, B and C). In contrast, deletion of the PHF domain in R3 (ΔPHF6-tau, Figure 2A) massively reduced both tau's bundling and stabilizing capacity (Figure 2, B–E, and Supplemental Movie S5). Thus, the two PHF domains are both involved in microtubule stabilization, and the domain located at the beginning of R3 plays a key role in microtubule bundling.

Differential tau phosphorylation promotes distinct microtubule organizations

Phosphorylation of tau is known to modulate its microtubule-binding and -stabilizing properties (Gendron and Petrucelli, 2009; Noble *et al*., 2013). Among the 40 phosphorylation sites identified to date, a few located within tau MTBD have been found to modulate tau's effect on microtubule dynamics, but none have been reported to affect its microtubule bundling function directly (Trinczek *et al*., 1995; Kiris *et al*., 2011). To investigate how phosphorylation of tau affects bundle assembly and behavior, we generated phosphorylation-mimicking glutamate mutants on specific sites located in distinct tau subdomains identified as major regulators of microtubule behavior (Gendron and Petrucelli, 2009; Noble *et al*., 2013; and the present work). These sites are phosphorylated under physiological conditions. The mutants produced were S46E/T69E/S113E (distal part of the projection domain), S175E/T181E (proximal part of the projection domain), S262E (first repeat of MTBD), S305E (adjacent to the PHF domain in R3), and S404E (C-terminal tail) (Figure 3A). All these mutants bound microtubules with a similar stoichiometry under self-assembly conditions at tau:tubulin molar ratios comparable to those used in TIRF-based assays (Supplemental Figure S2). Our results show that the S175E/S181E-tau mutant still stabilized microtubules (Figure 3B and Supplemental Table S2) and bundled them as efficiently as the unmodified 4R-tau (Figure 3, C and D). As previously reported (Trinczek *et al*., 1995; Kiris *et al*., 2011; Ramirez-Rios *et al*., 2016), S262E-tau mutant exhibited decreased microtubule-stabilizing activity compared with 4R-tau (more catastrophes, fewer rescues, and appearance of touch-and-run events, Figure 3, B and C, and Supplemental Table S2). However, our results indicate that this mutant could still cross-link microtubules (Figure 3, C and D) to produce dynamic microtubule bundles (Figure 3E and Supplemental Movie S6). In contrast, phosphomimicking mutations in the distal part of the projection domain (S46E/T69E/S113E), in the C-terminal tail (S404E), or in the vicinity of the PHF domain in R3 (S305E) had no significant impact on tau's capacity to stabilize microtubules (Figure 3B and Supplemental Table S2), but they did considerably reduce the frequency of polymer bundling, thus promoting the assembly of networks mostly made of single stable networked microtubules (Figure 3, C–E, and Supplemental Movie S6). Taken together, these results strongly suggest that phosphorylation of tau affects its capacity to either bundle or stabilize microtubules, leading to the formation of distinct microtubule organizations (Supplemental Movie S6).

Pathological mutations of tau increase the formation of dynamic microtubule bundles

Mutations in the tau gene have been identified in a particular type of neurodegenerative dementia known as frontotemporal dementia with Parkinsonism linked to chromosome 17 (FTDP-17) (Garcia and Cleveland, 2001; Ingram and Spillantini, 2002). These mutations either alter tau splicing, modifying the normal 1:1 ratio of 3R- to 4R-tau, or result in amino acid substitutions and deletions that generally impair tau's microtubule-stabilizing effect (Barghorn *et al*., 2000; Bunker *et al*., 2006; LeBoeuf *et al*., 2008; Elbaum-Garfinkle *et al*., 2014). To examine how FTDP-17 point mutations influence the ability of tau to organize microtubules, we generated recombinant forms of three different FTDP-17 tau mutants: ΔK280-tau, where the lysine residue located at the end of the PHF sequence in R2 was deleted; P301L-tau, which has a proline-to-leucine substitution in a conserved loop next to the PHF domain in R3 (Bergen *et al*., 2001; Kadavath *et al*., 2015); and V337M, containing a valine-to-methionine substitution in R4 (Figure 4A). Previous studies indicated that these mutants still interact with microtubules but have a compromised ability to regulate their assembly (Barghorn *et al*., 2000; LeBoeuf *et al*., 2008; Elbaum-Garfinkle *et al*., 2014). Under our TIRF-based assay conditions, all three mutants bound microtubules with a stoichiometry similar to that of 4R-tau (Supplemental Table S2). However, while V337M-tau behaved similarly to 4R-tau (Figure 4, B–D), the P301L and ΔK280 mutations altered both microtubule-bundling and -stabilizing properties of tau. These two mutants are poor microtubule stabilizers, and microtubules therefore undergo many catastrophes and very few rescues (Figure 4B). Simultaneously, these mutants increased the formation of microtubule bundles (Figure 4, C and D, and Supplemental Movie S7) by enhancing the probability of bundling per collision and promoting microtubule coalignments at significantly greater angles than with 4R-tau and V337M-tau. This effect was much greater with P301L-tau. This concomitant up-regulation of microtubule bundling and down-regulation of microtubule stability by tau mutants led to the formation of highly dynamic microtubule bundles. These data demonstrate that pathological mutations of tau can alter its ability to bundle and stabilize microtubules in opposing ways.

Tau proteins modify the lattice organization of growing microtubules

The differential effects of tau proteins on microtubule bundling could be explained by tau-induced changes of microtubule structure. Indeed, the ability of microtubules to undergo the bending deformations required for their coalignment and subsequent

bundling, depends on their mechanical properties, which are likely influenced by their lattice organization. For instance, an increase in protofilament number would stiffen microtubules (Gittes *et al.*, 1993; Kikumoto *et al.*, 2006), whereas local lattice defects, such as transitions in the number of protofilaments, may make microtubules more flexible (Portran *et al.*, 2013; Schaedel *et al.*, 2015). A recent study indicated that tau increases the average radius of prepolymerized taxol-stabilized microtubules (Choi *et al.*, 2009), but we still do not know how microtubules copolymerized with tau are organized. To gather information, we performed cryo–electron microscopy on microtubules that had been self-assembled in the presence of 4R-tau or some of the tau constructs described above. The constructs studied in these assays were chosen for their various effects on microtubule bundling. The images showed that, compared with the control population, which was mainly composed of 13-protofilament microtubules, all the tau constructs tested promoted the assembly of microtubules with 14 protofilaments (Figure 5, A and C). Small percentages of 15- and 16-profilament microtubules were also observed under these conditions. In addition, transitions in the number of protofilaments (e.g., from 13–14 protofilaments; double arrows in Figure 5, A and B) were observed along individual microtubules, producing local lattice defects. Such defects could be produced by end-to-end annealing of microtubules over time (Rothwell *et al.*, 1986) or directly generated during the microtubule elongation process (Chrétien and Fuller, 2000; Schaedel *et al.*, 2015). We do not favor the former hypothesis, because end-to-end annealing has been evidenced in mixtures of preformed stable microtubules (Rothwell *et al.*, 1986; de Forges *et al.*, 2016; Gramlich *et al.*, 2017), which is very different from our cryo–electron microscopy conditions (growing microtubules). The frequency of protofilament transitions was enhanced two- to fourfold in the presence of tau proteins and mutants over the control condition (Figure 5D). Overall, these data suggest that tau and the variants assayed in this study all generate similar lattice modifications during microtubule assembly, characterized by an increase in both protofilament number and protofilament transitions.

DISCUSSION

In recent years, substantial progress has been made in understanding how tau interacts with microtubules *via* its MTBD (Mukrasch *et al.*, 2009; Kadavath *et al.*, 2015). However, the mechanisms by which tau assembles linear microtubule bundles from dynamic polymers remain poorly understood. Using TIRF-based reconstitution assays, we were able to demonstrate that tau is an active bundler that promotes the coalignment and zippering of growing microtubules. Cryo–electron microscopy further revealed that tau changes the structure of microtubules during assembly by increasing the protofilament number and generating lattice defects. These modifications induced by tau might influence microtubule properties. Indeed, an increase in the protofilament number is assumed to stiffen microtubules (Gittes *et al.*, 1993; Kikumoto *et al.*, 2006), which may account for how tau promotes microtubule rigidity (Felgner *et al.*, 1997; Hawkins *et al.*, 2013). In contrast, lattice defects have been proposed to make microtubules more flexible (Janson and Dogterom, 2004; Schaedel *et al.*, 2015). How such opposite effects on microtubule mechanical properties could be related to the bundling process is unclear and will require further analysis. Strikingly, all of the tau forms tested in this study induced the same microtubule lattice changes regardless of their microtubule bundling efficiency. This suggests that the bundling efficiency of tau proteins depends on alternative microtubule-independent regulatory mechanisms related to the intrinsic properties of tau (see below).

Tau's projection domain is described as the main element responsible for microtubule bundling through complete dimerization (Rosenberg *et al.*, 2008; Feinstein *et al.*, 2016) or transient charge–charge attractions (Chung *et al.*, 2016), while the MTBD is considered to control microtubule dynamics (Brandt and Lee, 1993a; Trinczek *et al.*, 1995; Goode *et al.*, 1997). Surprisingly, our results indicated that a small fragment of tau, restricted to the repeat motifs, is sufficient to bundle microtubules with even stronger efficiency than that of full-length tau, suggesting an alternative bundling mechanism. One possible explanation for this observation is that basic C-terminal tau fragments stimulate microtubule bundling via electrostatic attraction between negatively charged microtubules, as suggested for cationic polyamines and more recently for N-terminally deleted forms of tau (Hamon *et al.*, 2011; Chung *et al.*, 2016). Conversely, as previously suggested (Choi *et al.*, 2009), the negative charges in the projection domain could decrease tau bundling efficiency by exerting a repulsive effect on adjacent microtubules. Our data are consistent with previous studies proposing a negative impact of the N-terminal domain of tau on its microtubule-based functions (Scott *et al.*, 1992; Brandt and Lee, 1993a; Zilka *et al.*, 2006; Derisbourg *et al.*, 2015). This strongly suggests that cleavage of tau's projection domain confers a gain of function on the protein. This gain of function might alter cytoskeleton and neuronal integrity in the brains of patients with Alzheimer's disease, where both N- and C-terminally truncated tau fragments have been identified (Wang *et al.*, 2010; Zilka *et al.*, 2012; Derisbourg *et al.*, 2015).

Unexpectedly, our results show that the C-terminal MTBD of tau, in addition to its microtubule-stabilizing role, also strongly influences the formation of microtubule bundles. We identified the two conserved PHF sequences located in the second and third repeats of the MTBD as key determinants for this regulation: both PHF sequences contribute to microtubule stabilization, whereas the sequence located in R3 also plays a major role in microtubule bundle assembly (Figure 6). The essential role of the two PHF domains in regulating microtubule dynamics is in line with their involvement in tau folding upon binding to the microtubule (Kadavath *et al.*, 2015) and in promoting microtubule self-assembly (Goode and Feinstein, 1994). We propose that local changes within (ΔK280-tau) or next to (S262E-tau, P301L-tau) the PHF sequences could modify how the MTBD interacts with microtubules, thereby altering tau's ability to stabilize microtubules while still bound to them (Supplemental Figure S2). These types of local perturbation of the MTBD conformation have recently been highlighted upon tau MTBD pseudophosphorylation (Schwalbe *et al.*, 2015). Furthermore, the PHF domain located in R3 plays a specific, and essential, role in microtubule coalignment, as shown by the facts that its deletion inhibits microtubule bundling, and that mutations located next to this domain (P301L, S305E) have a strong impact on microtubule bundling. If we assume that the microtubule-bundling mechanism involves complete dimerization (Rosenberg *et al.*, 2008; Feinstein *et al.*, 2016) or charge-charge attractions (Chung *et al.*, 2016) of the tau projection domain, our data suggest that the PHF sequence in R3 influences these interaction processes by modifying the overall conformation of the N-terminal part of tau. In line with this hypothesis, intramolecular contacts have been identified between the PHF sequence in R3 and the projection domain in soluble tau (Mukrasch *et al.*, 2009). Moreover, a very recent study proposed that microtubule-bound tau molecules in cells display a paperclip conformation with the N- and C-termini folding back onto the MTBD, which also supports a relationship between the MTBD and the projection domain of the tau molecule (Di Primio *et al.*, 2017).

Interestingly, phosphorylation and disease-related mutations of tau promoted distinct microtubule organizations by differentially

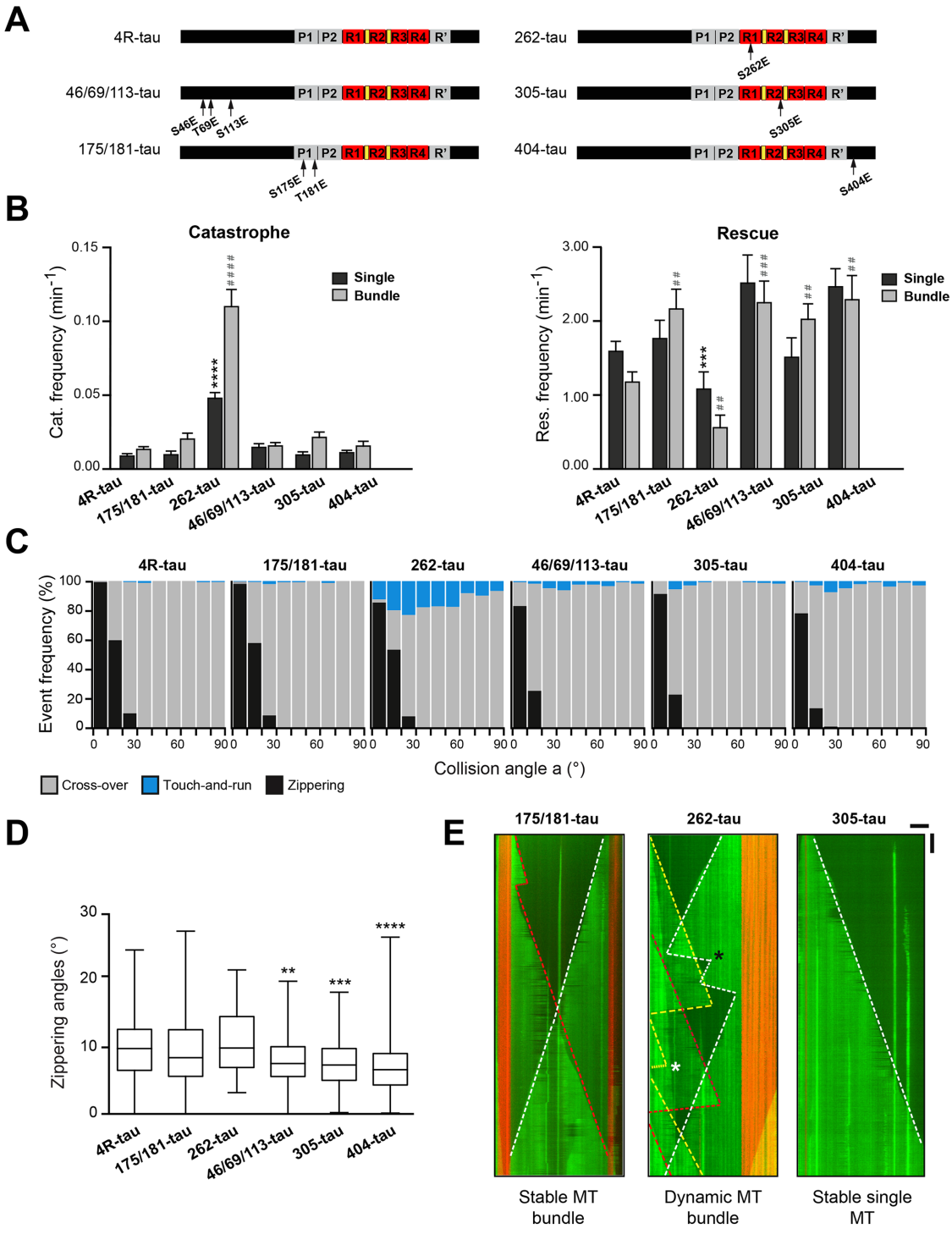

FIGURE 3: Site-specific pseudophosphorylation of tau differentially regulates its ability to bundle and stabilize microtubules. (A) Schematic representation of 4R-tau and the pseudophosphorylated mutants used in this study. In each tau mutant, specific serine or threonine residues were mutated to glutamate to mimic phosphorylation: S46, T69, and S113 in the distal part of the projection domain (46/69/113-tau); S175 and T181 in the proximal part of the projection domain (175/181-tau); S262 (262-tau) and S305 (305-tau) in the first and second repeats of the MTBD, respectively; and S404 in the C-terminal tail (404-tau). Arrows indicate the positions of amino acid substitutions. (B) Effects of tau phosphomutants on the frequency of catastrophes (left) and rescues (right) for single and bundled microtubules (see Supplemental Table S2 for detailed values). Microtubules were assembled from 10 μM tubulin in the presence of 100 nM 4R-tau or the tau phosphomutants. ***$p < 0.01$, ****$p < 0.0001$, ##$p < 0.01$, ###$p < 0.001$, ####$p < 0.0001$ (Kruskal–Wallis ANOVA followed by post hoc Dunn's multiple comparison). p values were calculated relative to single (*) or bundled (#) microtubules polymerized in the presence of 4R-tau. (C) Frequency distributions of crossover (gray), touch-and-run (blue), and zippering (black) events as a function of microtubule collision angles in the presence of tau phosphomutants. At least 200 collision events were analyzed for each condition. (D) Distribution of collision angles at

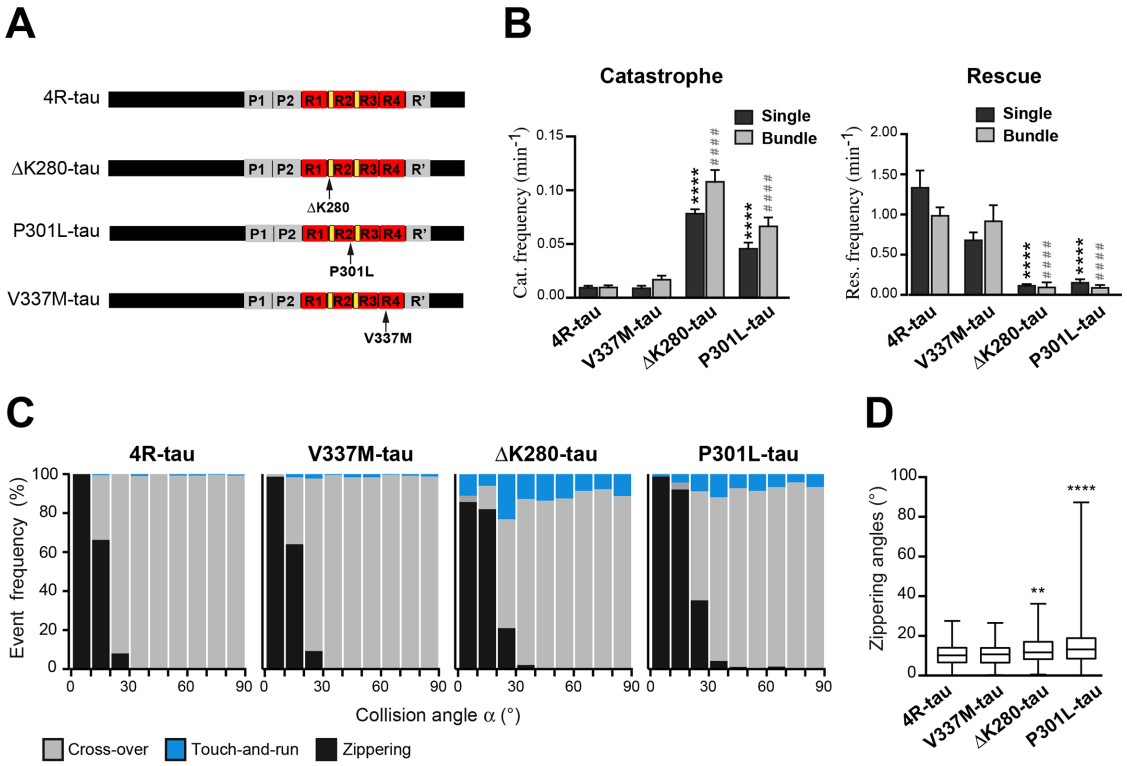

FIGURE 4: FTDP-17 mutant forms of tau exhibit enhanced microtubule bundling activity together with reduced microtubule-stabilizing effect. (A) Schematic representation of FTDP-17 tau mutants used in this study. Point mutations were located at the sites indicated. Domain details are as in Figure 1A. (B) Effects of tau mutants on the frequency of catastrophes (left) and rescues (right) for single and bundled microtubules (see Supplemental Table S3 for detailed values). Microtubules were assembled from 10 µM tubulin in the presence of 100 nM 4R-tau or tau FTDP-17 mutants. ****$p < 0.0001$, ####$p < 0.0001$ (Kruskal–Wallis ANOVA followed by post hoc Dunn's multiple comparison). p values were calculated relative to single (*) or bundled (#) microtubules polymerized in the presence of 4R-tau. (C) Frequency distributions for crossover (gray), touch-and-run (blue), and zippering (black) events as a function of microtubule collision angles in the presence of tau FTDP-17 mutants. At least 200 collision events were analyzed for each condition. (D) Distribution of collision angles at which microtubules coalign in the presence of 4R-tau and FTDP17 mutants. Boxes represent percentiles 25–75, and whiskers extend from the minimum to the maximum values. The horizontal lines inside boxes indicate median values. **$p < 0.01$, ****$p < 0.0001$ (Kruskal–Wallis ANOVA followed by post hoc Dunn's multiple comparison; the numbers of angles measured were 235, 166, 145, and 233 for 4R-, V337M-, ΔK280-, and P301L-tau, respectively). p values were calculated relative to the 4R-tau condition.

regulating microtubule bundling or stabilization (Figure 6). Mutations that impair tau-mediated microtubule stabilization were restricted to the MTBD (S262E-tau, ΔK280, P301L); those affecting tau-mediated microtubule bundling were located in various tau subdomains (projection domain, MTBD, and C-terminal tail). As suggested above, such site-dependent effects may involve modifications of how tau MTBD interacts with microtubules and/or how tau folds onto the microtubule surface. Consistently, tau pseudophosphorylation was reported to induce conformational changes of soluble tau, characterized by swinging movements of tau's projection domain and/or C-terminal tail (Jeganathan *et al.*, 2008). Mutations and phosphorylation within or next to tau MTBD have also been recently proposed to alter the global hairpin conformation of microtubule-bound tau molecules in cells (Di Primio *et al.*, 2017). These changes could affect tau–tau interaction and subsequent microtubule bundling. Overall, these results have important implications for the normal and pathological functions of tau. First, they strongly suggest that tau's capacity to distinctly regulate its microtubule-bundling and -stabilizing activities can be tightly controlled by its phosphorylation state and/or alternative splicing (4R vs. 3R). This newly identified balancing mechanism, illustrated in Figure 6, is essential for tau to generate distinct microtubule organizations,

which microtubules coalign in the presence of 4R-tau and tau phosphomutants. Boxes represent percentiles 25–75, and the whiskers extend from the minimum to the maximum values. The horizontal lines inside boxes indicate median values. **$p < 0.01$, ***$p < 0.001$, ****$p < 0.0001$ (Kruskal–Wallis ANOVA followed by post hoc Dunn's multiple comparison; the numbers of angles measured were 236, 207, 81, 110, 123, and 101 for 4R-, 175/181-, 262-, 46/69/113, 305-, and 404-tau, respectively). p values were calculated relative to the 4R-tau condition. (E) Kymograph examples of microtubules growing in the presence of three pseudophosphorylated tau forms (175/181-, 262-, and 305-tau) producing different microtubule populations. Dotted lines represent the growing extremities of microtubules. White and black asterisks indicate some catastrophe and rescue events, respectively. Horizontal scale bars: 10 µm; vertical scale bars: 3 min. MT, microtubules.

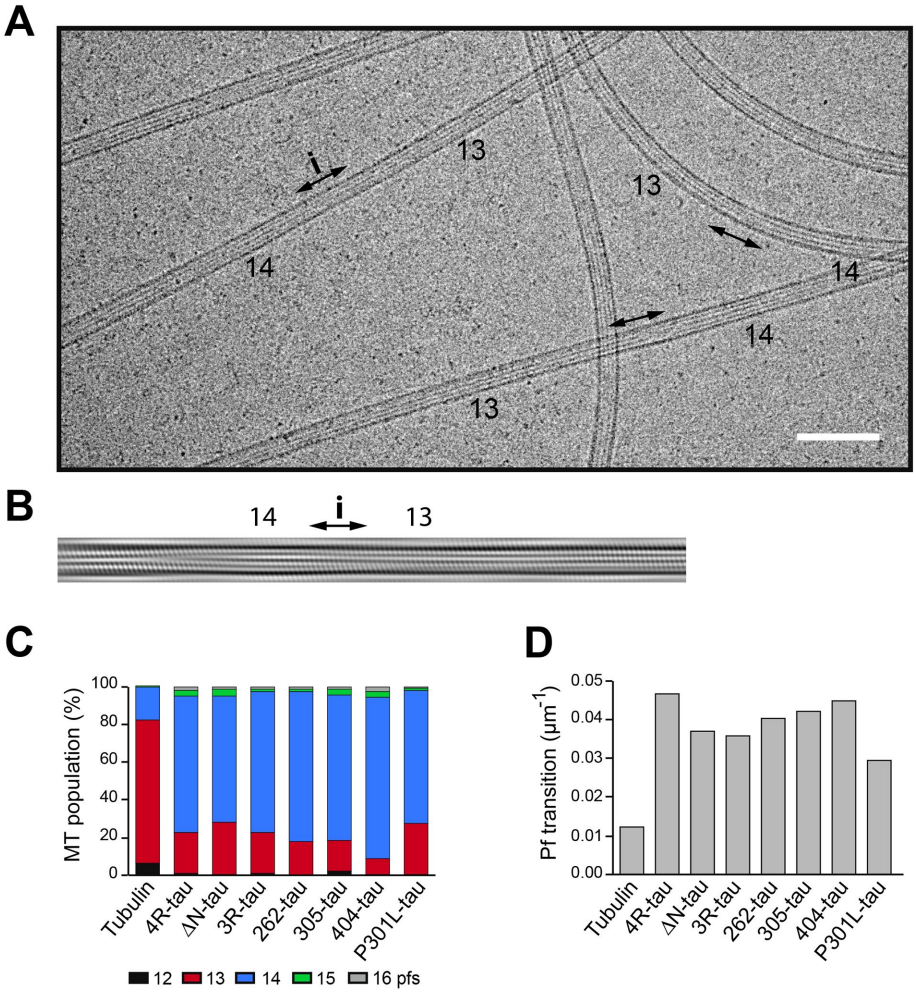

FIGURE 5: Tau proteins modify the microtubule lattice organization. (A) Cryo–electron microscopy image of microtubules assembled from tubulin in the presence of tau. The protofilament number is indicated below each microtubule and the protofilament transitions are shown by double arrows. Scale bar: 100 nm. (B) Filtered image of the transition from 14 to 13 protofilaments labeled in panel A (i). (C) Effect of tau proteins on the distribution of microtubules depending on their protofilament number (see color code). Microtubules were assembled with either tubulin alone (60 μM) or tubulin (20 μM) and various tau proteins (5 μM). Under these conditions, the initial growth rates determined by spin-down assays (see *Materials and Methods*) were comparable (2.56 ± 0.09, 2.09 ± 0.04, 2.18 ± 0.04, 2.38 ± 0.03, 2.47 ± 0.09, 2.13 ± 0.04, 2.25 ± 0.06, and 2.66 ± 0.04 μm·min^{-1} for tubulin alone, 4R-tau, ΔN-tau, 3R-tau, 262-tau, 305-tau, 404-tau and P301L-tau respectively). (D) Effect of tau proteins on the frequency of protofilament transitions.

which might play key roles in a number of microtubule-dependent neuronal functions such as axonal elongation, internal trafficking and maintenance (Kapitein and Hoogenraad, 2015; Voelzmann *et al.*, 2016). Second, our results provide further insights into how pathological tau modifications, such as disease-related increased phosphorylation levels or mutations, might alter microtubule organization by promoting the formation of specific networks (e.g., stable single microtubules or highly dynamic bundles). One prevailing view is that tau-related diseases are linked to detachment of tau from microtubules, leading to microtubule destabilization (Kolarova *et al.*, 2012). Our results appear to indicate an alternative situation where pathological forms of tau continue to bind to microtubules but misregulate their dynamic and/or bundling properties.

In conclusion, our results reveal novel mechanisms by which tau is able to switch microtubule network organization via the differential regulation of microtubule bundling and dynamics. We further provide evidence that nonphysiological modifications of tau can compromise one or both of these activities, leading to loss of function (reduced microtubule stability or bundling) and/or gain of function (increased microtubule bundling) effects. Taken together, these data strongly suggest an active role for nonaggregated pathological forms of tau in altering cytoskeleton properties. Our findings support the view that pathways other than tau aggregation and detachment from microtubules are involved in the progression of neurodegenerative diseases (Kolarova *et al.*, 2012; Kopeikina *et al.*, 2012) and might open up new perspectives on the development of novel therapeutic strategies.

MATERIALS AND METHODS

DNA constructs and reagents

Human tau isoforms containing one insert (N) and either three or four repeats (R) (3R- and 4R-tau, respectively) were used in this study. The following tau constructs were generated by a PCR-based strategy (amino acid numbering is given according to the longest 2N4R-tau isoforms): ΔN-tau and ΔNΔC-tau, corresponding to aa 198–441 and 244–400, respectively; 2R-tau, corresponding to the deletion of R2 and R3 (aa 275–336); ΔPHF6*-tau, ΔPHF6-tau and ΔPHF12-tau in which aa 275–280, 306–311, and both PHF sequences were deleted. Tau phosphomutants were generated by PCR using the QuickChange II XL site-directed mutagenesis kit (Agilent Technologies) to exchange serine or threonine for glutamic acid residues. A similar approach was used to produce FTDP17 mutants of tau. Most constructs were subcloned in the pDEST17 (Invitrogen) vector, except ΔN-tau and ΔNΔC-tau, which were subcloned in the pET-28a vector (Novagen).

Protein purification

His-tagged recombinant tau proteins were expressed in *Escherichia coli* strain BL21-DE3-pLysS (constructs cloned in pET-28a) or BL21-AI (constructs cloned in pDEST17) (Invitrogen). Expression of ΔN- and ΔNΔC-tau fragments was induced by adding 1 mM IPTG to the culture medium and incubating for 3 h at 37°C. Expression of the other tau forms was induced by overnight incubation with 0.2% L-arabinose at 18°C. Soluble proteins were extracted from cells in lysis buffer (40 mM Tris-HCl, 500 mM NaCl, protease inhibitor cocktail [Roche], pH 7.0) by three freeze/thaw cycles and sonication. Clarified lysates were mixed with Talon metal affinity resin (Clontech) for 1 h at 4°C in Buffer A (20 mM Tris-HCl, 500 mM NaCl, 10 mM imidazole, 0.1% Triton, pH 7.0). The resin was washed three times in buffer A before proteins were eluted with buffer A supplemented with 200 mM imidazole. Samples were further processed

by size-exclusion chromatography in BRB80 buffer (80 mM PIPES, 1 mM EGTA, 1 mM $MgCl_2$, pH 6.74). Purified proteins were concentrated and frozen in liquid nitrogen. Protein concentrations were determined by a Bradford assay using bovine serum albumin (BSA) as a standard.

Tubulin was purified from fresh bovine brain and fluorescently labeled with ATTO 488 and ATTO 565 (ATTO-TEC GmbH, Germany) or biotinylated according to Hyman *et al.* (1991).

TIRF microscopy

Microtubule seeds were obtained by polymerizing 10 µM tubulin (50% biotinylated tubulin and 50% ATTO 565–labeled tubulin) in the presence of 1 mM guanosine-5′-[(α,β)-methyleno]triphosphate (GMPCPP) in BRB80 at 35°C for 1 h. Microtubule seeds were then centrifuged for 5 min at 68,000 × *g*, resuspended in an equal volume of BRB80 supplemented with 1 mM GMPCPP, and stored in liquid nitrogen until needed.

Perfusion chambers were prepared with functionalized silane-PEG-biotin (Laysan Bio) coverslips and silane-PEG (Creative PEGworks) glass slides, as described previously (Portran *et al.*, 2013; Elie *et al.*, 2015) The flow cell was successively perfused with neutravidin (25 µg/ml in 1% BSA in BRB80) (Pierce), PLL-g-PEG (2 kD, 0.1 mg/ml in 10 mM HEPES, pH 7.4) (Jenkem), BSA (1% in BRB80 buffer), and microtubule seeds. Microtubule assembly was initiated from the seeds attached to the coverslip surface by injecting 10 µM tubulin (containing 30% ATTO 488–labeled tubulin) in the presence of 100 nM of the different tau proteins in TIRF assay buffer (4 mM dithiothreitol, 1% BSA, 50 mM KCl, 1 mg/ml glucose, 70 µg/ml catalase, 580 µg/ml glucose oxidase, 0.017% methylcellulose (1500 centipoise) in BRB80). Dual-color time-lapse images were recorded using an inverted Eclipse Ti microscope (Nikon) with an Apochromat 60 × 1.49 numerical aperture oil immersion objective (Nikon), equipped with an iLas[2] TIRF system (Roper Scientific) and a cooled charge-coupled device camera (EMCCD Evolve 512, Photometrics) controlled by MetaMorph 7.7.5 software (Molecular Devices). Fluorescence was excited using 491-and 561-nm lasers, and time-lapse imaging was performed at a rate of one frame per 5 s with an 80-ms exposure time for 45–60 min.

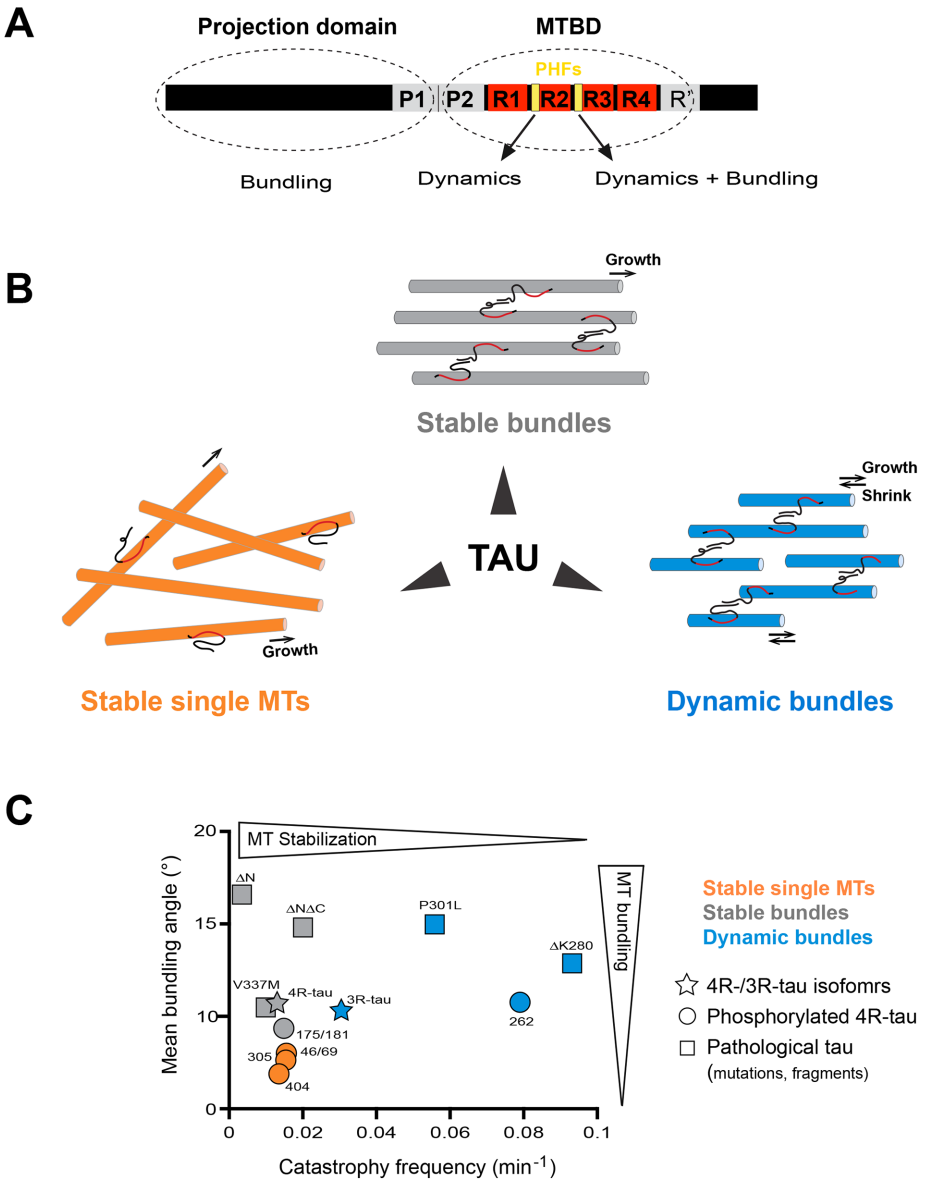

FIGURE 6: Tau switches microtubule network organizations depending on its physiological or pathological states. (A) Main tau subdomains involved in regulating microtubule bundling and dynamics. The projection domain is involved in microtubule bundling, whereas the two PHF domains influence both microtubule dynamics and bundling. (B) Schematic representation of the distinct microtubule organizations promoted by tau depending on its physiological or pathological modifications. (C) Microtubule bundling vs. stabilizing properties of tau proteins. The ability of tau proteins to bundle microtubules is estimated based on mean bundling angle; their ability to stabilize microtubules corresponds to the mean frequency of catastrophes. MTs, microtubules.

Microtubule bundling and dynamics analysis

Image analysis was performed using ImageJ (Schneider *et al.*, 2012). Microtubule dynamic parameters were determined on kymographs using an in-house KymoTool macro. Growth and shrinkage rates were calculated from the slopes of the microtubule growth and shrinkage phases. The catastrophe and rescue frequencies were determined by dividing the number of events per microtubule by the time spent in growing and shrinking states, respectively. The contact angles between microtubules upon collision were measured on the movie frames for each outcome (crossover, zippering, and touch-and-run). Event frequencies were calculated for 10° contact angle windows from 0° to 90°.

Measuring microtubule growth rate in self-assembly conditions used for cryo–electron microscopy experiments

Because microtubule growth rate has been proposed to influence the formation of lattice defects (Chrétien and Fuller, 2000; Janson and Dogterom, 2004; Schaedel *et al.*, 2015), cryo–electron microscopy

conditions were set up to get similar initial growth rates in the absence (control conditions) and in the presence of tau proteins. Microtubules were self-assembled from 60 µM tubulin (10% ATTO 488–labeled tubulin and 90% unlabeled tubulin) or 20 µM tubulin in the presence of 5 µM 4R-tau proteins in BRB80–50 mM KCL buffer supplemented with 1 mM GTP. Tubulin assembly was initiated at 35°C and assembly was stopped after 2 min by adding 1 ml of BRB80 containing 0.5% glutaraldehyde and 25% (wt/vol) sucrose. Microtubules were then centrifuged on coverslips for 20 min at 68,000 × *g* at 25°C before being fixed in ice-cold methanol (10 min at –20°C) and washed in PBS-Tween 0.1%. Microtubules were observed under an epifluorescence microscope. Using ImageJ software, the lengths of at least 100 microtubules were measured on each coverslip. Mean growth rates were determined from mean microtubule length measurements.

Cryo–electron microscopy

Vitreous-ice-embedded microtubules were prepared under a controlled atmosphere with constant temperature/humidity using the vitrification robot Vitrobot MARK IV (FEI). Microtubules were polymerized for at least 10 min at 35°C from 60 µM tubulin alone or a mix of 20 µM tubulin and 5 µM 4R-tau proteins. Samples (4 µl) were dropped onto holey carbon grids within the warm and humid chamber of the Vitrobot, blotted, and plunged into liquid ethane. Specimens were observed under low-dose conditions using a transmission electron microscope (FEI Tecnai F20 200 kV FEG) equipped with an FEI eagle 4K CCD camera.

Printed images were analyzed to determine microtubule lattice organization based on the specific moiré fringe pattern resulting from the two-dimensional projection of protofilaments (Wade *et al.*, 1990). Microtubules with 13 unskewed protofilaments display a continuous contrast image, whereas all other configurations produce images characterized by alternating fringe patterns that vary according to the protofilament number. Microtubule lengths were measured using an electronic ruler (Silva); these lengths then served to determine the proportions of the different microtubule populations. A total length of at least 300 µm was measured under each condition. Filtered images of microtubules were generated in ImageJ using Tubule J software provided by Denis Chrétien (Blestel *et al.*, 2009).

Statistics

All statistical analyses were performed using Prism 6 (GraphPad Software, USA).

ACKNOWLEDGMENTS

We thank Yasmina Saoudi and the imaging facility platform (PIC-GIN) for help with image acquisitions, Angélique Vinit, Emilie Couriol and Ninon Zala for help with protein purification. We thank Fiona Hemming and Fabrice Senger for critical reading of the manuscript. This work was supported by the CNRS/INSERM ATIP-Avenir program, the Agence Nationale pour la Recherche (ANR-2011-MALZ-001-02) and a cofinanced grant by the Union France Alzheimer et Maladies Apparentées and the Fédération pour la Recherche sur le Cerveau (FRC) (AAP SM 2015). E.P. was supported by PhD fellowships from the Ministère de l'Enseignement Supérieur et de la Recherche and the Fondation pour la Recherche Médicale (FDT20160435467). A.E. was supported by PhD fellowships from the Rhône-Alpes region (Program "Cible 2011") and the Fondation pour la Recherche Médicale (FDT20140930826). This work used the platforms at the Grenoble Instruct Center (ISBG: UMS 3518 CNRS-CEA-UJF-EMBL), which are supported from FRISBI (ANR-10-INSB-05-02) and GRAL (ANR-10-LABX-49-01) within the Grenoble Partnership for Structural Biology (PSB). The IBS electron microscope facility is supported by the Rhône-Alpes region, the Fonds Feder, and the Fondation pour la Recherche Médicale. We thank Maria Bacia and Emmanuelle Neumann, members of the IBS electron microscope facility, for their help.

REFERENCES

Alonso AC, Zaidi T, Grundke-Iqbal I, Iqbal K (1994). Role of abnormally phosphorylated tau in the breakdown of microtubules in Alzheimer disease. Proc Natl Acad Sci USA 91, 5562–5566.

Amos LA, Schlieper D (2005). Microtubules and maps. Adv Protein Chem 71, 257–298.

Barghorn S, Zheng-Fischhöfer Q, Ackmann M, Biernat J, von Bergen M, Mandelkow EM, Mandelkow E (2000). Structure, microtubule interactions, and paired helical filament aggregation by tau mutants of frontotemporal dementias. Biochemistry (Mosc) 39, 11714–11721.

Bergen M, Barghorn S, Li L, Marx A, Biernat J, Mandelkow E-M, Mandelkow E (2001). Mutations of tau protein in frontotemporal dementia promote aggregation of paired helical filaments by enhancing local β-structure. J Biol Chem 276, 48165–48174.

Binder LI, Frankfurter A, Rebhun LI (1985). The distribution of tau in the mammalian central nervous system. J Cell Biol 101, 1371–1378.

Blestel S, Kervrann C, Chrétien D (2009). A Fourier-based method for detecting curved microtubule centers: application to straightening of cryo-electron microscope images. In: Proceedings of the IEEE International Symposium on Biomedical Imaging: From Nano to Macro, Boston, MA: IEEE, 298–301.

Brandt R, Lee G (1993a). Functional organization of microtubule-associated protein tau: identification of regions which affect microtubule growth, nucleation, and bundle formation in vitro. J Biol Chem 268, 3414–3419.

Brandt R, Lee G (1993b). The balance between tau protein's microtubule growth and nucleation activities: implications for the formation of axonal microtubules. J Neurochem 61, 997–1005.

Bunker JM, Kamath K, Wilson L, Jordan MA, Feinstein SC (2006). FTDP-17 mutations compromise the ability of tau to regulate microtubule dynamics in cells. J Biol Chem 281, 11856–11863.

Chen J, Kanai Y, Cowan NJ, Hirokawa N (1992). Projection domains of MAP2 and tau determine spacings between microtubules in dendrites and axons. Nature 360, 674–677.

Choi MC, Raviv U, Miller HP, Gaylord MR, Kiris E, Ventimiglia D, Needleman DJ, Kim MW, Wilson L, Feinstein SC, *et al.* (2009). Human microtubule-associated-protein tau regulates the number of protofilaments in microtubules: a synchrotron X-ray scattering study. Biophys J 97, 519–527.

Chrétien D, Fuller SD (2000). Microtubules switch occasionally into unfavorable configurations during elongation. J Mol Biol 298, 663–676.

Chung PJ, Song C, Deek J, Miller HP, Li Y, Choi MC, Wilson L, Feinstein SC, Safinya CR (2016). Tau mediates microtubule bundle architectures mimicking fascicles of microtubules found in the axon initial segment. Nat Commun 7, 12278.

Cleveland DW, Hwo SY, Kirschner MW (1977a). Physical and chemical properties of purified tau factor and the role of tau in microtubule assembly. J Mol Biol 116, 227–247.

Cleveland DW, Hwo SY, Kirschner MW (1977b). Purification of tau, a microtubule-associated protein that induces assembly of microtubules from purified tubulin. J Mol Biol 116, 207–225.

Conde C, Cáceres A (2009). Microtubule assembly, organization and dynamics in axons and dendrites. Nat Rev Neurosci 10, 319–332.

de Forges H, Pilon A, Cantaloube I, Pallandre A, Haghiri-Gosnet A-M, Perez F, Poüs C (2016). Localized mechanical stress promotes microtubule rescue. Curr Biol 26, 3399–3406.

Derisbourg M, Leghay C, Chiappetta G, Fernandez-Gomez FJ, Laurent C, Demeyer D, Carrier S, Buée-Scherrer V, Blum D, Vinh J, *et al.* (2015). Role of the tau N-terminal region in microtubule stabilization revealed by new endogenous truncated forms. Sci Rep 5, 9659.

Di Primio C, Quercioli V, Siano G, Rovere M, Kovacech B, Novak M, Cattaneo A (2017). The distance between N and C termini of tau and of FTDP-17 mutants is modulated by microtubule interactions in living cells. Front Mol Neurosci 10, 210.

Drechsel DN, Hyman AA, Cobb MH, Kirschner MW (1992). Modulation of the dynamic instability of tubulin assembly by the microtubule-associated protein tau. Mol Biol Cell 3, 1141–1154.

Elbaum-Garfinkle S, Cobb G, Compton JT, Li X-H, Rhoades E (2014). Tau mutants bind tubulin heterodimers with enhanced affinity. Proc Natl Acad Sci USA 111, 6311–6316.
Elie A, Prezel E, Guérin C, Denarier E, Ramirez-Rios S, Serre L, Andrieux A, Fourest-Lieuvin A, Blanchoin L, Arnal I (2015). Tau co-organizes dynamic microtubule and actin networks. Sci Rep 5, 9964.
Feinstein HE, Benbow SJ, LaPointe NE, Patel N, Ramachandran S, Do TD, Gaylord MR, Huskey NE, Dressler N, Korff M, *et al.* (2016). Oligomerization of the microtubule-associated protein tau is mediated by its N-terminal sequences: implications for normal and pathological tau action. J Neurochem 137, 939–954.
Felgner H, Frank R, Biernat J, Mandelkow EM, Mandelkow E, Ludin B, Matus A, Schliwa M (1997). Domains of neuronal microtubule-associated proteins and flexural rigidity of microtubules. J Cell Biol 138, 1067–1075.
Fitzpatrick AWP, Falcon B, He S, Murzin AG, Murshudov G, Garringer HJ, Crowther RA, Ghetti B, Goedert M, Scheres SHW (2017). Cryo-EM structures of tau filaments from Alzheimer's disease. Nature 547, 185–190.
Garcia ML, Cleveland DW (2001). Going new places using an old MAP: tau, microtubules and human neurodegenerative disease. Curr Opin Cell Biol 13, 41–48.
Gendron TF, Petrucelli L (2009). The role of tau in neurodegeneration. Mol Neurodegener 4, 13.
Gittes F, Mickey B, Nettleton J, Howard J (1993). Flexural rigidity of microtubules and actin filaments measured from thermal fluctuations in shape. J Cell Biol 120, 923–934.
Goedert M, Jakes R (1990). Expression of separate isoforms of human tau protein: correlation with the tau pattern in brain and effects on tubulin polymerization. EMBO J 9, 4225–4230.
Goode BL, Denis PE, Panda D, Radeke MJ, Miller HP, Wilson L, Feinstein SC (1997). Functional interactions between the proline-rich and repeat regions of tau enhance microtubule binding and assembly. Mol Biol Cell 8, 353–365.
Goode BL, Feinstein SC (1994). Identification of a novel microtubule binding and assembly domain in the developmentally regulated inter-repeat region of tau. J Cell Biol 124, 769–782.
Gramlich MW, Conway L, Liang WH, Labastide JA, King SJ, Xu J, Ross JL (2017). Single molecule investigation of kinesin-1 motility using engineered microtubule defects. Sci Rep 7, 44290.
Gustke N, Trinczek B, Biernat J, Mandelkow EM, Mandelkow E (1994). Domains of tau protein and interactions with microtubules. Biochemistry (Mosc) 33, 9511–9522.
Hamon L, Savarin P, Curmi PA, Pastré D (2011). Rapid assembly and collective behavior of microtubule bundles in the presence of polyamines. Biophys J 101, 205–216.
Hawkins TL, Sept D, Mogessie B, Straube A, Ross JL (2013). Mechanical properties of doubly stabilized microtubule filaments. Biophys J 104, 1517–1528.
Himmler A, Drechsel D, Kirschner MW, Martin DW (1989). Tau consists of a set of proteins with repeated C-terminal microtubule-binding domains and variable N-terminal domains. Mol Cell Biol 9, 1381–1388.
Hoogenraad CC, Bradke F (2009). Control of neuronal polarity and plasticity—a renaissance for microtubules?. Trends Cell Biol 19, 669–676.
Hyman A, Drechsel D, Kellogg D, Salser S, Sawin K, Steffen P, Wordeman L, Mitchison T (1991). Preparation of modified tubulins. Methods Enzymol 196, 478–485.
Ingram EM, Spillantini MG (2002). Tau gene mutations: dissecting the pathogenesis of FTDP-17. Trends Mol Med 8, 555–562.
Janson ME, Dogterom M (2004). A bending mode analysis for growing microtubules: evidence for a velocity-dependent rigidity. Biophys J 87, 2723–2736.
Jeganathan S, Hascher A, Chinnathambi S, Biernat J, Mandelkow E-M, Mandelkow E (2008). Proline-directed pseudo-phosphorylation at AT8 and PHF1 epitopes induces a compaction of the paperclip folding of Tau and generates a pathological (MC-1) conformation. J Biol Chem 283, 32066–32076.
Kadavath H, Jaremko M, Jaremko Ł, Biernat J, Mandelkow E, Zweckstetter M (2015). Folding of the tau protein on microtubules. Angew Chem Int Ed Engl 54, 10347–10351.
Kapitein LC, Hoogenraad CC (2015). Building the neuronal microtubule cytoskeleton. Neuron 87, 492–506.
Kikumoto M, Kurachi M, Tosa V, Tashiro H (2006). Flexural rigidity of individual microtubules measured by a buckling force with optical traps. Biophys J 90, 1687–1696.
Kiris E, Ventimiglia D, Sargin ME, Gaylord MR, Altinok A, Rose K, Manjunath BS, Jordan MA, Wilson L, Feinstein SC (2011). Combinatorial tau pseudophosphorylation: markedly different regulatory effects on microtubule assembly and dynamic instability than the sum of the individual parts. J Biol Chem 286, 14257–14270.
Kolarova M, García-Sierra F, Bartos A, Ricny J, Ripova D (2012). Structure and pathology of tau protein in Alzheimer disease. Int J Alzheimers Dis 2012, 731526.
Kopeikina KJ, Hyman BT, Spires-Jones TL (2012). Soluble forms of tau are toxic in Alzheimer's disease. Transl Neurosci 3, 223–233.
LeBoeuf AC, Levy SF, Gaylord M, Bhattacharya A, Singh AK, Jordan MA, Wilson L, Feinstein SC (2008). FTDP-17 mutations in tau alter the regulation of microtubule dynamics: an "alternative core" model for normal and pathological tau action. J Biol Chem 283, 36406–36415.
Lee G, Neve RL, Kosik KS (1989). The microtubule binding domain of tau protein. Neuron 2, 1615–1624.
Mitchison T, Kirschner M (1984). Dynamic instability of microtubule growth. Nature 312, 237–242.
Mukrasch MD, Bibow S, Korukottu J, Jeganathan S, Biernat J, Griesinger C, Mandelkow E, Zweckstetter M (2009). Structural polymorphism of 441-residue tau at single residue resolution. PLoS Biol 7, e34.
Mukrasch MD, von Bergen M, Biernat J, Fischer D, Griesinger C, Mandelkow E, Zweckstetter M (2007). The "jaws" of the tau-microtubule interaction. J Biol Chem 282, 12230–12239.
Noble W, Hanger DP, Miller CCJ, Lovestone S (2013). The importance of tau phosphorylation for neurodegenerative diseases. Front Neurol 4, 83.
Panda D, Goode BL, Feinstein SC, Wilson L (1995). Kinetic stabilization of microtubule dynamics at steady state by tau and microtubule-binding domains of tau. Biochemistry (Mosc) 34, 11117–11127.
Panda D, Samuel JC, Massie M, Feinstein SC, Wilson L (2003). Differential regulation of microtubule dynamics by three- and four-repeat tau: implications for the onset of neurodegenerative disease. Proc Natl Acad Sci USA 100, 9548–9553.
Portran D, Zoccoler M, Gaillard J, Stoppin-Mellet V, Neumann E, Arnal I, Martiel JL, Vantard M (2013). MAP65/Ase1 promote microtubule flexibility. Mol Biol Cell 24, 1964–1973.
Ramirez-Rios S, Denarier E, Prezel E, Vinit A, Stoppin-Mellet V, Devred F, Barbier P, Peyrot V, Sayas CL, Avila J, *et al.* (2016). Tau antagonizes end-binding protein tracking at microtubule ends through a phosphorylation-dependent mechanism. Mol Biol Cell 27, 2924–2934.
Rosenberg KJ, Ross JL, Feinstein HE, Feinstein SC, Israelachvili J (2008). Complementary dimerization of microtubule-associated tau protein: Implications for microtubule bundling and tau-mediated pathogenesis. Proc Natl Acad Sci USA 105, 7445–7450.
Rothwell SW, Grasser WA, Murphy DB (1986). End-to-end annealing of microtubules in vitro. J Cell Biol 102, 619–627.
Schaedel L, John K, Gaillard J, Nachury MV, Blanchoin L, Théry M (2015). Microtubules self-repair in response to mechanical stress. Nat Mater 14, 1156–1163.
Schneider CA, Rasband WS, Eliceiri KW (2012). NIH Image to ImageJ: 25 years of image analysis. Nat Methods 9, 671–675.
Schwalbe M, Kadavath H, Biernat J, Ozenne V, Blackledge M, Mandelkow E, Zweckstetter M (2015). Structural impact of tau phosphorylation at threonine 231. Struct Lond Engl 1993 23, 1448–1458.
Scott CW, Klika AB, Lo MM, Norris TE, Caputo CB (1992). Tau protein induces bundling of microtubules in vitro: comparison of different tau isoforms and a tau protein fragment. J Neurosci Res 33, 19–29.
Trinczek B, Biernat J, Baumann K, Mandelkow EM, Mandelkow E (1995). Domains of tau protein, differential phosphorylation, and dynamic instability of microtubules. Mol Biol Cell 6, 1887–1902.
Voelzmann A, Hahn I, Pearce SP, Sánchez-Soriano N, Prokop A (2016). A conceptual view at microtubule plus end dynamics in neuronal axons. Brain Res Bull 126, 226–237.
Wade RH, Chrétien D, Job D (1990). Characterization of microtubule protofilament numbers. How does the surface lattice accommodate? J Mol Biol 212, 775–786.
Wang Y, Garg S, Mandelkow E-M, Mandelkow E (2010). Proteolytic processing of tau. Biochem Soc Trans 38, 955–961.
Weingarten MD, Lockwood AH, Hwo SY, Kirschner MW (1975). A protein factor essential for microtubule assembly. Proc Natl Acad Sci USA 72, 1858–1862.
Zilka N, Filipcik P, Koson P, Fialova L, Skrabana R, Zilkova M, Rolkova G, Kontsekova E, Novak M (2006). Truncated tau from sporadic Alzheimer's disease suffices to drive neurofibrillary degeneration in vivo. FEBS Lett 580, 3582–3588.
Zilka N, Kovacech B, Barath P, Kontsekova E, Novák M (2012). The self-perpetuating tau truncation circle. Biochem Soc Trans 40, 681–686.